This article has been accepted for inclusion in a future issue of this journal. Content is final as presented, with the exception of pagination.

Cooperative Control for Ocean Sampling: The Glider Coordinated Control System

Derek A. Paley, *Member, IEEE*, Fumin Zhang, *Member, IEEE*, and Naomi Ehrich Leonard, *Fellow, IEEE*

***Abstract*—The Glider Coordinated Control System (GCCS) uses a detailed glider model for prediction and a simple particle model for planning to steer a fleet of underwater gliders to a set of coordinated trajectories. The GCCS also serves as a simulation testbed for the design and evaluation of multivehicle control laws. In this brief, we describe the GCCS and present experimental results for a virtual deployment in Monterey Bay, CA and a real deployment in Buzzards Bay, MA.**

***Index Terms*—Distributed control, marine technology, mobile robots, ocean sampling, sensor networks, underwater vehicles.**

I. Introduction

EFFECTIVE monitoring of the ocean enables oceanographers to make new discoveries that improve our understanding of the environment. An emerging method for sustained ocean monitoring is automatic and coordinated control of autonomous sensor platforms such as underwater gliders. Autonomous underwater gliders are small, unmanned submersibles characterized by reliability and endurance. In a typical glider deployment, multiple gliders survey a region of interest for weeks or months in order to sample the ever-changing ocean processes with adequate frequency in space and time. Feedback controls that coordinate the glider sampling trajectories to optimally distribute measurements increase the collective survey performance [1]. To meet this objective, we have designed the Glider Coordinated Control System (GCCS), which builds on previous experience with real-time glider coordination [2].

The GCCS also serves as a simulation testbed for development of coordinated control algorithms. Simulated, or virtual, gliders operate in realistic ocean fields that are provided as input. Accordingly, it is possible to use the GCCS to explore and test solutions to many of the challenges that come with controlling a network of gliders in the ocean. A strong, variable flow field, which, at times, can be stronger than the forward speed of a glider, is one such challenge. Other challenges include long delays in feedback, uncertainty in communication, and asynchronicity in feedback and communication [2]. Because a number of these challenges have not yet been fully addressed by theoretical methods, the GCCS as testbed plays an indispensable role in development.

The GCCS is designed to support operation of an autonomous ocean sampling network (AOSN) [3]. These networks leverage advances in underwater robot technology to perform ocean surveys with unprecedented resolution. Since the inception of the AOSN concept, there have been several demonstrations of (remote) control systems for multiple underwater vehicles. The Glider Mission Control Center, an agent-based software system designed for manual and automated control of underwater gliders, has been demonstrated in multivehicle operations in the New York Bight and west coast Florida shelf [4]. The Fleet Logistical Interface and Control Software, developed to coordinate multivehicle missions such as formation control of micro-unmanned underwater vehicles (UUVs), was tested in Newport River on the coast of North Carolina [5]. The Autonomous Systems Monitoring and Control has controlled a solar-powered underwater vehicle in Lake George, NY [6]. In addition, semiautonomous underwater vehicle (AUV) coordination with manual assistance is increasingly common [7].

Our contribution, which we describe in this brief, is to design and demonstrate at sea an automated control system that performs feedback control at the level of the fleet. The GCCS differs from other multi-AUV control systems because it uses feedback control laws to automate fleet coordination. Since the time scale of the fleet motion is much slower than the time scale of the individual dynamics, we decouple the fleet trajectory design from the individual trajectory tracking. We address the trajectory design problem in [8]–[11] using decentralized feedback control of a simplified model of glider motion. Here, we address how the GCCS steers a fleet of gliders to a set of coordinated trajectories by combining the simple model with a detailed model of glider dynamics. We further demonstrate the practical use and merit of the GCCS by describing experimental results from a recent virtual deployment in Monterey Bay, CA, and a real ocean deployment in Buzzards Bay, MA.

In Section II, we review ocean sampling with underwater gliders and describe our approach for enabling collective motion of a glider fleet using cooperative control algorithms. In Section III, we describe the automated control system that implements these algorithms. In Section IV, we provide experimental results from two glider deployments.

II. Problem Background and Approach

A. Ocean Sampling With Underwater Gliders

Autonomous underwater gliders soar through the ocean on a pair of fixed wings using an efficient, buoyancy-driven propul-

Manuscript received November 2, 2006; revised April 2, 2007. Manuscript received in final form July 25, 2007. Recommended by Associate Editor C. Rabbath. This work was supported in part by the U.S. Office of Naval Research (ONR) under Grants N00014-02-1-0826, N00014-02-1-0861, and N00014-04-1-0534. The work of D. Paley was supported by the National Science Foundation (NSF) Graduate Research Fellowship, the Princeton Wu Graduate Fellowship, and the Pew Charitable Trust under Grant 2000-002558.

D. A. Paley is with the Department of Aerospace Engineering, University of Maryland, College Park, MD 20742 USA (e-mail: dpaley@umd.edu).

F. Zhang is with the School of Electrical and Computer Engineering, Georgia Institute of Technology, Savannah, GA 31407 USA (e-mail: fumin@ece.gatech.edu).

N. E. Leonard with the Department of Mechanical and Aerospace Engineering, Princeton University, Princeton, NJ 08544 USA (e-mail: naomi@princeton.edu).

Digital Object Identifier 10.1109/TCST.2007.912238

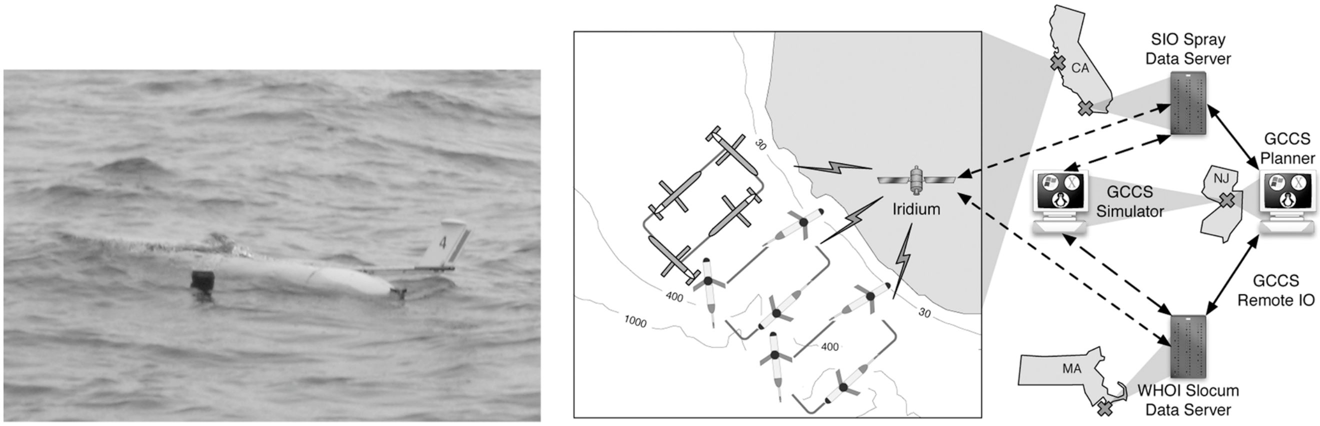

(a) (b)

Fig. 1. (a) Slocum glider *we04* in Buzzards Bay. While on the surface, the vehicle tail, which houses antennas for satellite communication, is elevated by an internal air bladder to achieve better reception. (b) The GCCS system architecture. The three main components of the GCCS are the planner, the simulator, and the remote input/output (I/O). The glider data servers, which are located in Woods Hole, MA, and La Jolla, CA, connect via Iridium satellite communication to the gliders as they periodically come to the surface (shown here in Monterey Bay, CA).

sion system [7], [12]. The Slocum glider shown in Fig. 1(a) is manufactured by Webb Research Corporation and operated by the Woods Hole Oceanographic Institution (WHOI), Woods Hole, MA. Another underwater glider, the Spray, is manufactured and operated by the Scripps Institution of Oceanography (SIO), La Jolla, CA. Gliders such as the Slocum and the Spray move vertically in the water by cyclically changing their buoyancy with a hydraulic pump. They convert their vertical velocity to horizontal "roller-coaster" motion by controlling their pitch to generate lift from a pair of fixed wings. Gliders steer either by moving an internal mass to roll and turn or by controlling an external rudder. Although they travel at low speeds (0.2–0.3 m/s) relative to propeller-driven underwater vehicles (which travel at 1–3 m/s), gliders are capable of much longer deployments (2–10 weeks versus 12–36 h).

Gliders periodically surface to connect via satellite or radio frequency communication to computers on shore as illustrated in Fig. 1(b). It is also possible to equip gliders with acoustic modems to communicate over short distances underwater. While on the surface, gliders transmit measured data and receive new waypoints, which are the coordinates of their next destinations. Gliders use a Global Position System (GPS) receiver to determine their position and to estimate the (depth-averaged) ocean currents encountered during the previous dive.

During deployments, gliders autonomously sample ocean properties such as temperature, salinity, and optical backscatter at depths up to 1500 m. The design of glider sampling trajectories often maximizes a metric such as model predictive skill [13] or minimizes a metric determined by objective analysis (OA) mapping error [14]. Minimization of OA mapping error can be obtained through coordinated control of a glider fleet [1]. Computing the OA mapping error requires an *a priori* description of the covariance of fluctuations around the mean of a scalar field, which is parameterized by the spatial and temporal decorrelation lengths of the field. OA provides an estimate for the average of the field using a linear combination of sensor measurements (if an *a priori* description of the mean is available). It also provides the residual uncertainty of this estimate, the mapping error, which reflects the quality of sampling performance.

One of the sampling performance metrics used below is the average of the OA mapping error over the sampling domain. This metric, called the average error, is minimized by collecting samples that are separated in space and time by the decorrelation lengths of the scalar field of interest. Samples that are spaced more closely may be redundant, whereas samples that are spaced more widely may introduce gaps in coverage. The decorrelation lengths are determined by what is being sampled; however, only the locations in space and time of the samples (not the sampled values) impact performance.

B. Glider Coordinated Trajectories

In the GCCS, feedback control laws stabilize collective motion of a simple glider model to a set of coordinated trajectories. We design this set of trajectories, the glider coordinated trajectories (GCT), to achieve the ocean–science objectives of the glider deployment, such as minimization of the average error. We adapt the GCT in the event of glider failure, in response to changing ocean currents, or to meet evolving scientific objectives. In typical deployments, gliders travel around closed curves in order to take measurements along long, repeated transects. The GCT specifies the desired track for each glider as well as the coordination and spacing between the gliders on their tracks. We refer to the spacing between gliders on the same track as the relative curve phase [11]. If two or more gliders travel around the same track, then they may maintain a fixed distance from each other (measured along the track). For example, if two gliders stay on opposite sides of the track, then their relative curve phase is π. If two or more gliders travel around different but similarly sized tracks, then they may synchronize their orbits so that the relative curve phase is zero. The GCT specifies whether each glider's control effort is dedicated to steering around its assigned track or to a balance of steering to the track and steering to coordinate with other gliders.

This article has been accepted for inclusion in a future issue of this journal. Content is final as presented, with the exception of pagination.

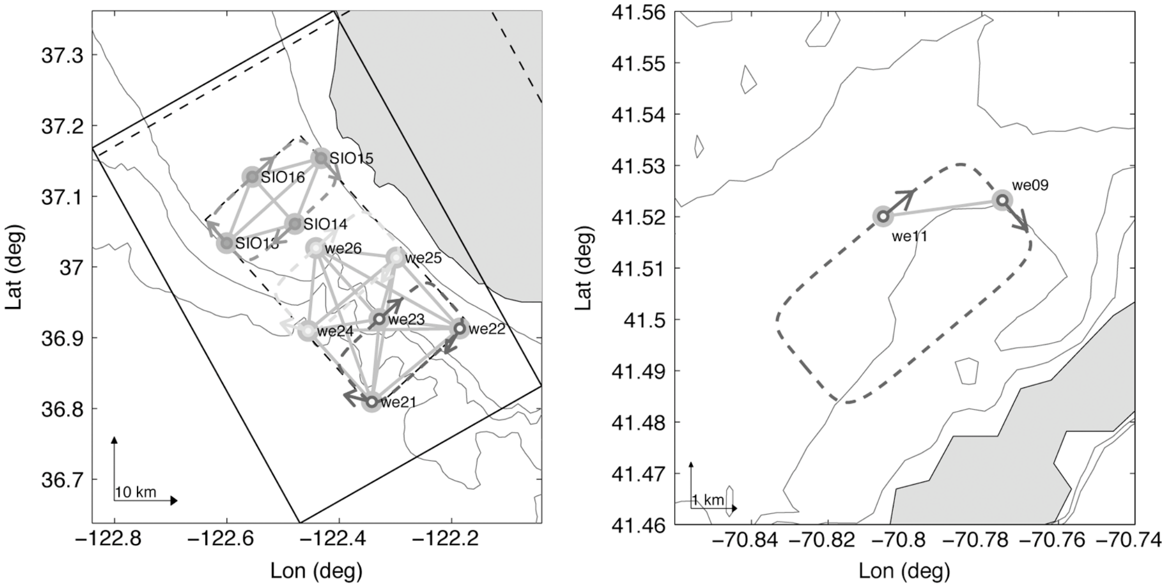

(a) (b)

Fig. 2. Sample GCTs. Glider tracks are dashed gray lines and the coordination links are solid lines connecting the gliders. (a) GCT, Monterey Bay. Four Spray gliders (labeled "SIO") travel clockwise around the 10 km × 20 km northern track and maintain uniform separation on the track. Three Slocum gliders (labeled "we") travel clockwise around the middle track and three more around the southern track; each set of three maintains uniform separation on each track. In addition, the Slocum gliders on the middle and southern tracks synchronize with one another. (b) GCT, Buzzard Bay. Two gliders travel clockwise around a 2.8 km × 5.6 km rectangular track and maintain along-track separation of 1/6 the curve perimeter.

An essential aspect of designing GCTs is choosing the interconnection topology for glider coordination. The interconnection topology determines which pairs of gliders are coupled for planning purposes. The trajectories of coupled gliders are planned jointly and depend on their relative position and direction of motion. Because gliders do not necessarily come to the surface at the same time, they are not configured to communicate directly with one another (interglider communication is implicitly performed by the GCCS). Nonetheless, the interconnection topology is described by a graph whose nodes represent gliders and whose edges represent (bidirectional) coordination. For example, we illustrate in Fig. 2(a) the GCT and corresponding coordination graph for ten gliders in Monterey Bay. This GCT is designed to keep gliders uniformly separated on tracks in order to achieve low average error inside and on the 20 km × 40 km bounding box (black dashed line). In order to achieve this objective, the six gliders in the middle and southern tracks form three pairs of synchronized gliders. A second GCT is shown in Fig. 2(b), in which two gliders in Buzzards Bay travel clockwise around a 2.8 km × 5.6 km rectangular track and maintain an along-track separation of 1/6 the curve perimeter.

III. Coordinated Control System Design

The GCCS is a modular, cross-platform software suite written in MATLAB®. It implements feedback control laws for coordination of a glider fleet. The three main modules of the GCCS are the planner, which is the real-time controller, the simulator, which serves as control testbed, and the remote input/output (I/O) module, which interfaces to gliders indirectly through the glider data servers [see Fig. 1(b)]. To plan trajectories for the gliders, which surface asynchronously, the GCCS uses two different models: 1) a detailed glider model with flow that is integrated to estimate glider motion and 2) a simple glider model, called the particle model, that is integrated to compute desired trajectories (with or without coordinated control). We refer to the software that integrates these two models as the glider integrator and particle integrator, respectively.

A. System Architecture

Glider Planner: The glider planner encapsulates the multi-vehicle control algorithm [see block diagram in Fig. 3(a)]. The planner uses the glider model to predict glider motion underwater and the particle model to plan future glider trajectories. The planned trajectories originate from the position and time of the next expected surfacing of each glider. The interplay between the glider model and the particle model is fundamental to the execution of a coordination algorithm. The implementation of a new coordination algorithm is facilitated by the existence of a well-defined interface between the particle model and the coordinated controller.

Planning new trajectories for all gliders occurs simultaneously. We call the sequence of steps that produces new glider trajectories a planning cycle. A planning cycle starts whenever a glider surfaces and ends when the planner generates new waypoints for all gliders. Due to operational concerns like glider speed and boat traffic, a glider does not wait on the surface—where it drifts passively—for its new waypoints. Instead, each glider uses the most recent set of waypoints that were computed before it surfaced. The planning cycle executes immediately after a glider surfaces, because new waypoints for all gliders are computed whenever a single glider surfaces.

For each glider that has surfaced since the last planning cycle, the planner calculates inaccuracies in the predictions of effective speed, expected surface position, and expected surface time.

This article has been accepted for inclusion in a future issue of this journal. Content is final as presented, with the exception of pagination.

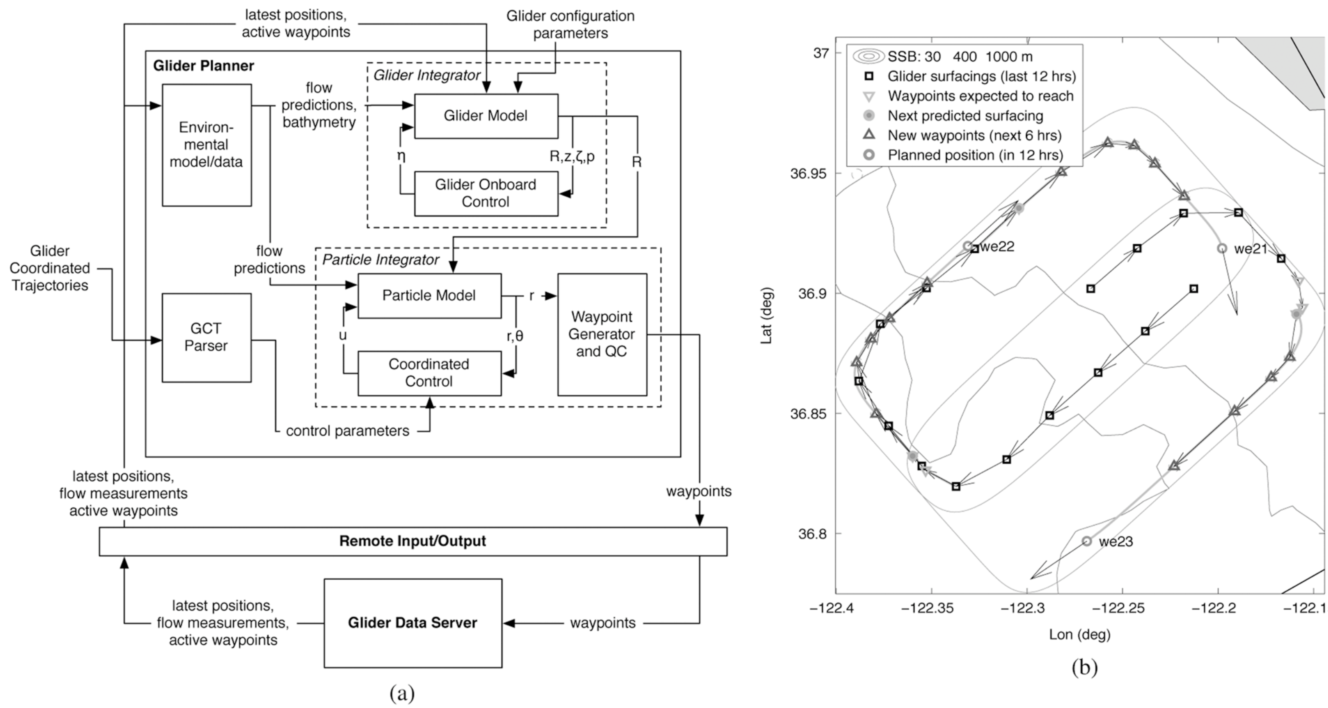

Fig. 3. GCCS glider planner. (a) Glider planner feedback loop. The planner creates waypoints to steer the fleet to a GCT by integrating the glider model for prediction and the particle model for planning. The glider planner interfaces to the glider data server(s) via the remote I/O module. (b) Glider planner graphical output. Trajectories for three Slocum gliders "we21," "we22," and "we23." The planned trajectories (thin solid lines) originate at each glider's next expected surface location (filled circles) and terminate at the 12–h planning horizon (open circles). Also shown are the bathymetry (water depth) contours 30, 400, and 1000 m.

Prediction errors are useful for gauging glider and planner performance. The planner uses the glider model as described below to predict each glider's underwater trajectory and next surfacing location and time. As input to the glider model, the planner computes a surface and underwater flow forecast by fusing all recent glider flow measurements using OA. In the next step in the planning cycle, described in detail below, the planner integrates the particle model to generate planned trajectories. The planner converts the planned trajectory of each glider to a list of waypoints, which must pass a quality control filter (QC). Surfacing when expected is one requirement to pass QC and failure to do so serves as an indication of potential problems with the glider or the glider data server. Fig. 3(b) illustrates the output of a planning cycle produced by the GCCS for monitoring.

Glider Simulator: In addition to providing a real-time controller, the GCCS serves as a simulation testbed for glider coordinated control algorithms. We also use the glider simulator during a glider deployment to predict glider motion in ocean flow forecasts. A central advantage is the ability to test strategies in the presence of strong flow and communication and feedback constraints and uncertainties, challenges that are not yet fully addressed by theoretical methods. The glider simulator uses the glider model to predict glider motion. To predict the motion of a coordinated fleet of gliders, we run the glider simulator in tandem with the glider planner. The software interface between the glider planner and simulator is identical to the interface between the glider planner and the real gliders, and the simulated gliders produce the same data files as the real gliders. These features enable use of the GCCS, in conjunction with a virtual ocean model, to conduct virtual experiments.

Remote I/O: Robust networking enables the GCCS to run automatically. The remote I/O module supports communication over the Internet between the glider planner and glider simulator as well as between the glider planner and the glider data servers. In addition, the remote I/O module publishes real-time planner status for monitoring and supervision of the GCCS as shown in Fig. 3(b). To support timely operator intervention, the remote I/O module sends e-mail notification of software or operational errors.

B. Glider Integrator

A central component of both the glider planner and simulator is the glider integrator, used to predict glider trajectories in the ocean. Predicting glider trajectories is critical to glider planning because new trajectories are generated while gliders are underwater. We model the motion of each glider and its onboard control system under the influence of the bathymetry (water depth) and currents (water velocity). The bathymetry is important because gliders maintain a minimum altitude above the bottom. Ocean currents are important because they advect gliders and also because gliders respond to their onboard current estimates. The glider onboard control system integrates its position, which is called the "dead-reckoned position," from estimates of its horizontal speed and heading. The GCCS predicts both glider position and glider dead-reckoned position; these differ if, for example, the planner uses a more accurate flow estimate than the glider.

The glider model is a discrete-time, 3-D, kinematic model of glider motion subject to the glider onboard pitch, heading, and

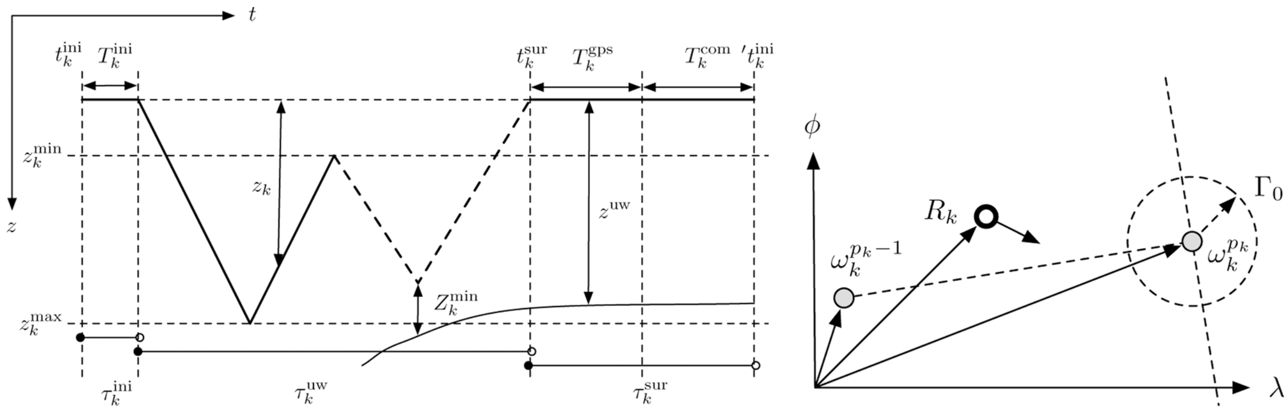

(a) (b)

Fig. 4. Notation for the glider model. (a) Glider model coordinates. Coordinates for time t and depth z during a single dive, which progresses from left to right: t_k^{ini} is the dive initialization time, t_k^{sur} is the surface time, and $'t_k^{\mathrm{ini}}$ is the time at which the next dive initializes. (b) Waypoint completion conditions. The glider position R_k, previous waypoint $\omega_k^{p_k-1}$, and current waypoint $\omega_k^{p_k}$ in geodetic coordinates, where λ and ϕ represent longitude and latitude, respectively. The glider satisfies the radius waypoint condition by entering the dashed circle of radius Γ_0 centered at the current waypoint $w_k^{p_k}$. The finish line condition is satisfied when the glider crosses the dashed line through the current waypoint.

buoyancy control. The second-order transient effects of the onboard control are not modeled. We assume a fixed vertical speed and glide angle (pitch angle plus angle of attack) for both ascent and descent. Gliders move at constant speed in the direction of their desired headings and are advected by a 3-D flow field. We separate the equations of motion for the three phases of a single dive: on the surface before the dive (dive initialization), underwater during the dive, and on the surface after the dive.

We describe the glider model using the notation illustrated in Fig. 4(a). The gliders are labeled by the integers $k \in \{1, \ldots, N\}$, where N is the number of gliders. Let $t \geq 0$ represent absolute time in the glider integrator. We denote the time step and discrete-time step index by $\triangle t \in \mathbb{R}^+$ and $n \in \mathbb{Z}$, respectively. The superscript $^{\mathrm{sur}}$ (resp., $^{\mathrm{uw}}$) refers to surface (resp., underwater). For glider k, let z_k denote depth, $z_k^{\min}$ denote minimum inflection depth (the shallowest depth at which the glider switches from ascending to descending), $z_k^{\max}$ denote maximum inflection depth, $Z_k^{\min}$ denote minimum altitude, and z^{uw} denote bathymetry. Also, for glider k, let t_k^{ini} denote dive initialization time, t_k^{sur} denote dive surface time, T_k^{ini} denote predive surface duration, T_k^{gps} denote postsurface GPS duration, and T_k^{com} denote communication duration. Last, let $\tau_k^{\mathrm{ini}} = [t_k^{\mathrm{ini}}, t_k^{\mathrm{ini}} + T_k^{\mathrm{ini}})$ denote the time interval before glider k dives, $\tau_k^{\mathrm{uw}} = [t_k^{\mathrm{ini}} + T_k^{\mathrm{ini}}, t_k^{\mathrm{sur}})$ denote during the dive, and $\tau_k^{\mathrm{sur}} = [t_k^{\mathrm{sur}}, t_k^{\mathrm{sur}} + T_k^{\mathrm{gps}} + T_k^{\mathrm{com}})$ denote after the dive. For convenience, we denote the end of interval τ by $\bar{\tau}$.

We use the ellipsoid E to model the earth shape. The glider integrator uses geodetic coordinates $R_k = (\lambda_k, \phi_k) \in E$ for the position of the kth glider, where λ_k and ϕ_k are latitude and longitude, respectively. Let $\Gamma : E \times E \to \mathbb{R}^+$ and $\eta : E \times E \to S^1$ be functions for computing distance and azimuth on the earth (not described here).

Position: The kth glider position R_k at time $t \geq t_k^{\mathrm{ini}}$ is the solution to the following discrete-time model, which depends on the position R_k, depth z_k, and waypoint index $p_k \in \mathbb{N}$. We denote the p_kth waypoint by $\omega_k^{p_k} \in E$. Let $f_k \in \mathbb{R}^2$ be the horizontal component of the kth glider velocity with respect to an earth-fixed frame.

1) Before the dive, $t \in \tau_k^{\mathrm{ini}} = [t_k^{\mathrm{ini}}, t_k^{\mathrm{ini}} + T_k^{\mathrm{ini}})$, and
$$R_k(n+1) = R_k(n) + f_k^{\mathrm{sur}}(R_k(n))\triangle t$$
where $n = 1, \ldots, \lfloor t - t_k^{\mathrm{ini}}/\triangle t\rfloor$, $R_k(1)$ is the position of the glider at t^{ini}, and f^{sur} is the total surface velocity.
2) During the dive, $t \in \tau_k^{\mathrm{uw}} = [t_k^{\mathrm{ini}} + T_k^{\mathrm{ini}}, t_k^{\mathrm{sur}})$, and
$$R_k(n+1) = R_k(n) + f_k^{\mathrm{uw}}(R_k(n), z_k(n), p_k(n))\triangle t$$
where $n = \lfloor \bar{\tau}_k^{\mathrm{ini}}/\triangle t\rfloor, \ldots, \lfloor t - t_k^{\mathrm{ini}}/\triangle t\rfloor$ and f^{uw} is the total velocity underwater.
3) After the dive, $t \in \tau_k^{\mathrm{sur}} = [t_k^{\mathrm{sur}}, t_k^{\mathrm{sur}} + T_k^{\mathrm{gps}} + T_k^{\mathrm{com}})$, and
$$R_k(n+1) = R_k(n) + f_k^{\mathrm{sur}}(R_k(n))\triangle t$$
where $n = \lfloor \bar{\tau}_k^{\mathrm{uw}}/\triangle t\rfloor, \ldots, \lfloor t - t_k^{\mathrm{ini}}/\triangle t\rfloor$.

Because the gliders have no propulsion on the surface, the glider surface velocity f^{sur} is equal to the flow velocity. Flow velocity on the surface is estimated using measured displacement of the glider between sequential GPS fixes. The horizontal component f^{uw} of the glider total velocity underwater, which is the sum of the horizontal glider velocity relative to the flow and the estimated horizontal flow velocity, depends on the ocean currents and the glider onboard control system. We compute the horizontal glider speed relative to the flow using the desired vertical speed and glide angle. We assume that the orientation of the horizontal glider velocity equals the desired heading of the glider, which is determined by the onboard control system and depends on the glider estimate of the flow. The onboard control algorithms are proprietary and not described here.

To determine the glider waypoint number $p_k(n)$, we integrate from the starting waypoint number using
$$p_k(n+1) = \begin{cases} p_k(n) + 1, & \text{if} \quad \Psi(R_k(n), p_k(n)) \\ p_k(n), & \text{otherwise} \end{cases}$$
where $\Psi(R_k(n), p_k(n))$ is a boolean waypoint completion condition. For example, the radius waypoint condition shown in Fig. 4(b) is $\Psi^{\mathrm{cir}}(R_k(n), p_k(n)) \triangleq \Gamma(R_k(n), \omega_k^{p_k(n)}) < \Gamma_0$, where $\Gamma_0 \in \mathbb{R}^+$ is the radius of a vertical cylinder centered at

the waypoint. In the presence of strong flow, the radius waypoint condition, combined with a heading algorithm that steers the glider directly toward the waypoint, can result in the glider turning into the flow. An alternate waypoint completion condition, the finish line condition, is satisfied if the glider crosses the line that passes through the current waypoint and is perpendicular to the line connecting the previous and current waypoints.

Depth: While underwater, gliders make either a single descent and ascent or continuously descend and ascend until the maximum dive duration $T_k^{\max}$ elapses. Although both configurations are used in practice, the (latter) roller-coaster motion minimizes time spent on the surface where the glider is vulnerable to surface currents and boats. Let g^{uw} be the vertical component of the glider total velocity. We denote the dive direction by $\zeta_k \in \{-1, +1\}$, where $+1$ represents descent. The kth glider depth at time t is the solution to the following discrete-time model, which depends on the position R_k, depth z_k, and dive direction ζ_k.

1) Before the dive, $t \in \tau_k^{\mathrm{ini}}$, and

$$z_k(n) = 0, \quad n = 1, \ldots, \left\lfloor \frac{t - t_k^{\mathrm{ini}}}{\triangle t} \right\rfloor.$$

2) During the dive, $t \in \tau_k^{\mathrm{uw}}$, and

$$z_k(n+1) = z_k(n) + g_k^{\mathrm{uw}}(R_k(n), z_k(n), \zeta_k(n))\triangle t$$

where $n = \lfloor \bar{\tau}_k^{\mathrm{ini}}/\triangle t \rfloor, \ldots, \lfloor t - t_k^{\mathrm{ini}}/\triangle t \rfloor$ and g^{uw} is the vertical component of the glider velocity.

3) After the dive, $t \in \tau_k^{\mathrm{sur}}$, and

$$z_k(n) = 0, \quad n = \left\lfloor \frac{\bar{\tau}_k^{\mathrm{uw}}}{\triangle t} \right\rfloor, \ldots, \left\lfloor \frac{t - t_k^{\mathrm{ini}}}{\triangle t} \right\rfloor.$$

The vertical component g^{uw} of the glider velocity is the sum of the glider vertical velocity relative to the flow and the estimated vertical flow velocity (if available). We compute the dive direction $\zeta_k \in \{-1, 1\}$ by integrating from the initial condition $\zeta_k(1) = 1$ using $\zeta_k(n+1) = -1$ if $(z_k(n) > z_k^{\max}) \cup (t > T_k^{\max}) \cup (z_k(n) > z^{\mathrm{uw}}(R_k(n)) - Z_k^{\min})$; $\zeta_k(n+1) = 1$ if $(z_k(n) < -\zeta_k(n) z_k^{\min}) \cup (t < T_k^{\max})$; and $\zeta_k(n+1) = \zeta_k(n)$, otherwise. In words, the glider ascends if it exceeds its maximum inflection depth, it exceeds the maximum dive duration, or its altitude is less than the minimum allowable altitude. If the glider is ascending before the end of the maximum dive duration, the dive direction reverses when the glider is shallower than the minimum inflection depth.

C. Particle Integrator

At the core of the glider planner is the particle integrator, which generates the glider planned trajectories using closed-loop (coordinated) control of the particle model. In this section, we quickly review the particle model and several coordinated control laws. Then, we present the particle integration algorithm, which is complicated by the fact that gliders surface asynchronously and do not wait on the surface for new waypoints. As a result, one or more gliders has recently surfaced and all gliders are underway at the start of particle trajectory integration.

Particle Model: Integrating the closed-loop particle model with state feedback generates the glider planned trajectories. In the particle model, gliders are represented by point masses (particles) confined to a horizontal plane. The motion of each particle obeys second-order Newtonian dynamics. The applied force, determined by the control input, is assumed to be perpendicular to the particle direction of motion. Consequently, the particles travel at constant speed and are steered by the control. The particle speed is the effective horizontal speed of the glider, which is the horizontal speed of the glider (relative to the flow) scaled by the fraction of time spent underwater, i.e., $T^{\max}/(T^{\max} + T^{\mathrm{ini}} + T^{\mathrm{gps}} + T^{\mathrm{com}})$. Alternative models of the particles moving in a flow field have been used. The design of coordinating control laws for gliders in the presence of strong flow is the subject of ongoing work.

As in the glider model, we index the particles by $k \in \{1, \ldots, N\}$, where N denotes the number of particles. Let $r_k = x_k + iy_k \in \mathbb{C} \equiv \mathbb{R}^2$ be the particle position and $\dot{r}_k = s_k e^{i\theta_k}$ be the particle velocity, where $s_k \in \mathbb{R}$ and $\theta_k \in \mathbb{T} \equiv S^1$ are the particle speed and direction of motion, respectively. Assuming each particle has unit mass, Newton's second law yields

$$\ddot{r}_k = \frac{d}{dt}(s_k e^{i\theta_k}) = \dot{s}_k e^{i\theta_k} + s_k \dot{\theta}_k i e^{i\theta_k} = (\nu_k + s_k u_k i) e^{i\theta_k}$$

where we have introduced the thrust $\nu_k = \dot{s}_k \in \mathbb{R}$ and (gyroscopic) steering $u_k = \dot{\theta}_k \in \mathbb{R}$ control inputs. By assumption, $\nu_k = 0$ and $s_k = s_0 < 0$ for all k. The equations of motion of the particle model are

$$\begin{aligned} \dot{r}_k &= s_0 e^{i\theta_k} \\ \dot{\theta}_k &= u_k, \qquad k = 1, \ldots, N. \end{aligned}$$

We use bold to represent the vectors $\mathbf{u} = (u_1, \ldots, u_N)^T, \mathbf{r} = (r_1, \ldots, r_N)^T$, and $\theta = (\theta_1, \ldots, \theta_N)^T$.

In the case $u_k = 0$, we have $\theta_k(t) = \theta_k(0)$, and each particle moves in a straight line along its initial heading. If $u_k = \omega_0 s_0 \neq 0$, then $\theta_k(t) = \theta_k(0) + \omega_0 s_0 t$, and each particle moves around a circle with radius $|\omega_0|^{-1}$. The center of the circle orbited by particle k is $c_k = r_k + i\omega_0^{-1} e^{i\theta_k}$. A feedback control law presented in [8] drives all particles to orbit the same circle such that $c_k = c_j$ for all pairs j and k. We call this particle configuration a circular formation. Symmetric circular formations are circular formations in which the particles are arranged in symmetric patterns as they travel around the circle. A feedback control law that isolates symmetric circular formations such as the splay state, in which the particles are uniformly spaced around the circle, is also provided in [8]. We have extended these results to the setting in which interparticle communication is limited, directed, and time-varying [9]. Furthermore, we have derived control algorithms that stabilize formations on multiple loops like the rounded rectangles suitable for oceanographic sampling [10], [11]. These controls use curvature and arc-length separation of particles along the desired loop as feedback.

During each planning cycle, the particle integrator coordinates particles that represent gliders on the surface with particles that represent gliders underwater. The particle integrator takes as input the trajectory predicted for each glider by the glider

TABLE I
PARTICLE INTEGRATOR ALGORITHM

Goal:	Integrate feedback control algorithm using asynchronous initial conditions.
Inputs:	Predicted trajectories up to next expected surfacing, desired tracks and coordination (GCT)
Outputs:	New waypoints for all gliders

During every planning cycle, the particle integrator performs:

1: set the integration start time t_0 to most recent glider actual surface time, $t_0 = \max_{k=1,\ldots,N} t_k^{\mathrm{sur}}$
2: **for** each particle $k = 1, \ldots, N$, set initial positions $r_k(t_0)$ to glider (surface) position at time ${}'t_k^{\mathrm{sur}}$, **end for**
3: **for** each particle $k = 1, \ldots, N$, set initial headings $\theta_k(t_0)$ according to control-specific algorithm, **end for**
4: call ODE solver with initial conditions $\mathbf{r}(t_0)$ and $\boldsymbol{\theta}(t_0)$ and time span $t \in [t_0, t_0 + T]$
The following pseudo-code is executed every iteration of the ODE solver
for each particle $k = 1, \ldots, N$,
5: **if** $t < {}'t_k^{\mathrm{sur}}$, set position $r_k(t)$ and heading $\theta_k(t)$ to glider predicted underwater position and heading, **end if**
end for
6: compute steering control $\dot{\boldsymbol{\theta}}(t) = \mathbf{u}(t)$ and particle velocity $\dot{\mathbf{r}}(t)$ using $\mathbf{r}(t)$ and $\boldsymbol{\theta}(t)$
for each particle $k = 1, \ldots, N$
7: **if** $t < {}'t_k^{\mathrm{sur}}$, set steering control $\dot{\theta}_k(t)$ and particle velocity $\dot{r}(t)$ to zero, **end if**
end for
8: **for** each particle, overwrite start of planned trajectory with predicted trajectory up to expected surface time, **end for**
9: **for** each particle, *generate waypoints* for $r_k(t)$, $t > {}'t_k^{\mathrm{sur}}$, and run *quality control*, **end for** (see text)

integrator as well as the desired tracks and coordination specified in the GCT. The output of the particle integrator is a new set of waypoints for each glider. The particle integrator uses a MATLAB® ODE solver to integrate trajectories from the time t_0 of the most recent glider surfacing to the planning horizon t_0+T. The initial position of each particle is the position of the glider at the next expected surfacing location and time ${}'t_k^{\mathrm{sur}}$. We choose the initial heading to maximize the convergence rate of the control.

For each glider k that is predicted to have not yet surfaced by time t, we set the corresponding particle position $r_k(t)$ and heading $\theta_k(t)$ to the predicted underwater position and heading. Then, the coordinated control algorithm computes the steering controls $\mathbf{u}(t)$ and velocities $\dot{\mathbf{r}}(t)$ for all particles using $\mathbf{r}(t)$ and $\boldsymbol{\theta}(t)$. For each glider k that is predicted to have not yet surfaced by t, we set the steering control $u_k(t)$ and velocity $\dot{r}_k(t)$ to zero. After the ODE solver computes the planned trajectories, we replace the portion of each trajectory that occurs before the next expected surface time with the predicted underwater trajectory. A pseudocode description is provided in Table I.

Waypoint Generation and Quality Control Filter: We convert the glider planned trajectories to waypoints and verify the waypoints using QC. There are two alternate waypoint generation methods. In the first method, the waypoints are spaced uniformly in time (assuming constant glider effective speed). In the second method, we convert portions of the planned trajectory with lower (resp., higher) curvature to fewer (resp., more) waypoints subject to a maximum (resp., minimum) spacing constraint. The latter method clusters waypoints near tight turns and spreads out waypoints along straight portions of the planned glider trajectories. To provide robustness to delays and errors incurred in satellite communication between the glider data server and the glider, each waypoint file that passes QC has a unique message number and an expiration date.

Waypoint quality control is required for safe, automated operation of gliders. To pass QC, the following criteria must be met: 1) the last glider position update must not be too old; 2) all waypoints other than those at the start of the list must be inside a prescribed bounding box; 3) waypoints must not be shallower than the glider minimum operating depth; and 4) waypoints must be spaced by no more (resp., less) than the maximum (resp., minimum) allowable spacing. We remove waypoints that are too shallow. Failure to meet any requirement other than 3) results in rejection of the entire waypoint list.

IV. EXPERIMENTAL RESULTS

We present results from two glider deployments in which the GCCS controlled multiple gliders to coordinated trajectories. These experiments further justify our approach to coordinated control of a glider fleet. First, we describe a virtual deployment in Monterey Bay in which the GCCS coordinated ten gliders in a rectangular domain, illustrated in Fig. 2(a). In this deployment, the GCCS also simulated the glider motion in a model ocean. Second, we describe a real deployment in Buzzards Bay in which the GCCS coordinated two gliders to motion around a single rectangular track, shown in Fig. 2(b).

A. Virtual Glider Deployment in Monterey Bay

The GCCS controlled ten gliders in a two-week-long virtual deployment in Monterey Bay in March 2006. The deployment was part of a virtual pilot experiment for the August 2006 Adaptive Sampling and Prediction (ASAP) field experiment [15]. The ocean science focus of the ASAP field experiment is to gain a better understanding of the 3-D ocean dynamics off Point

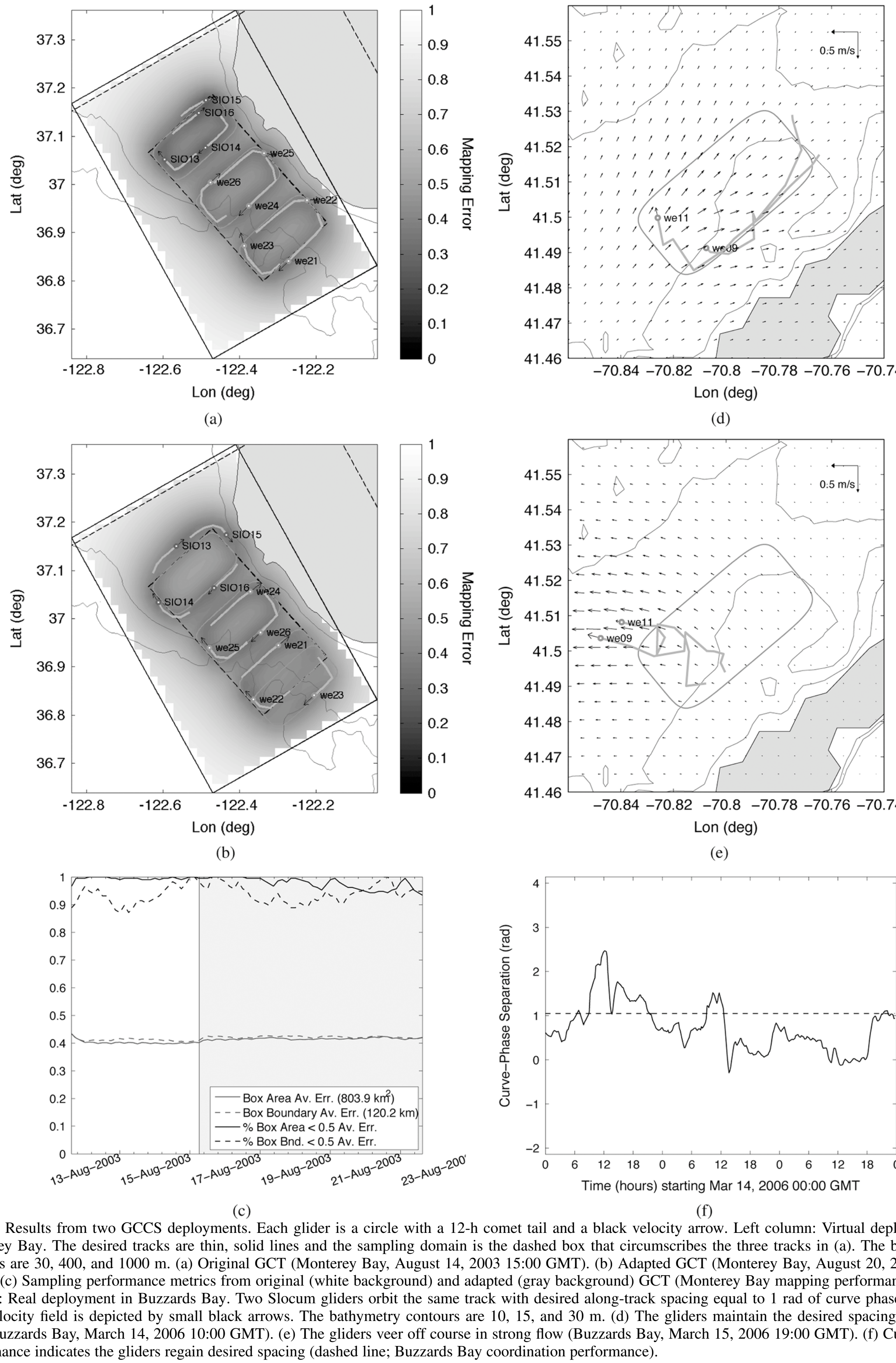

Fig. 5. Results from two GCCS deployments. Each glider is a circle with a 12-h comet tail and a black velocity arrow. Left column: Virtual deployment in Monterey Bay. The desired tracks are thin, solid lines and the sampling domain is the dashed box that circumscribes the three tracks in (a). The bathymetry contours are 30, 400, and 1000 m. (a) Original GCT (Monterey Bay, August 14, 2003 15:00 GMT). (b) Adapted GCT (Monterey Bay, August 20, 2003 11:00 GMT). (c) Sampling performance metrics from original (white background) and adapted (gray background) GCT (Monterey Bay mapping performance). Right column: Real deployment in Buzzards Bay. Two Slocum gliders orbit the same track with desired along-track spacing equal to 1 rad of curve phase. The OA flow velocity field is depicted by small black arrows. The bathymetry contours are 10, 15, and 30 m. (d) The gliders maintain the desired spacing in benign flow (Buzzards Bay, March 14, 2006 10:00 GMT). (e) The gliders veer off course in strong flow (Buzzards Bay, March 15, 2006 19:00 GMT). (f) Curve-phase performance indicates the gliders regain desired spacing (dashed line; Buzzards Bay coordination performance).

Año Nuevo, which is north of Santa Cruz, CA, by conducting a high-resolution survey with a fleet of underwater gliders and other (manned) assets. Of special interest to ASAP oceanographers is computing the mass and heat flux through the boundary of a 20 km $\times$ 40 km control volume. The virtual deployment tested the capability of the GCCS to: 1) control a glider fleet according to a candidate sampling plan and 2) respond to adaptations of this plan. We describe the initial sampling plan, the glider coordinated trajectories, in Section II-B [see Fig. 2(a)]. The control algorithm appears in [11].

During the virtual deployment, the gliders sampled a model ocean generated by the Harvard Ocean Prediction System from data collected during the 2003 Autonomous Ocean Sampling Network (AOSN-II) field experiment [16]. The model ocean contains temperature, salinity, and 3-D flow velocity at 500-m horizontal resolution with 22 vertical levels over a 35-day period starting August 6, 2003. The temperature data, which was collected by gliders during AOSN-II, has spatial and temporal temperature decorrelation lengths of 22 km and 2.2 days, respectively [12]. We used the decorrelation lengths to compute the OA mapping error and average error.

During the deployment, four virtual Spray gliders travelled clockwise around the northern track and sought uniform separation as shown in Fig. 5(a) and (b). Initially, the Spray gliders performed (simulated) Iridium communication after every dive. The resulting frequent and lengthy surfacings, combined with surface currents of 0.15–0.35 m/s, resulted in a low effective speed of 0.2 m/s (median value for all four Spray gliders). In addition, the strong surface currents degraded the glider along-track spacing. On the fourth day of the deployment, we reconfigured the Spray gliders to communicate on surfacing only if two or more hours had elapsed since the last communication. In this configuration, the glider effective speed increased by 25% to 0.25 m/s and the along-track separation recovered. We show the glider trajectories before [Fig. 5(a)] and after [Fig. 5(b)] the reconfiguration.

The group of six virtual Slocum gliders formed two synchronized subgroups of three gliders each, as shown in Fig. 5(a) and (b). During the deployment, the GCCS achieved good spacing of the Slocum subgroups around each track and good synchronization of the two subgroups. On the fourth day, we added a new track that extends outside the sampling domain to the south and overlaps the original southernmost track. This adaptation increases the sampling effort in a region south of the sampling domain without compromising the average error in the original domain. A so-called "scout" Slocum glider orbited the new track in coordination with the other Slocums. Fig. 5(b) shows that this adaptation did not degrade coordination. That is, if one superimposes the original and new southern tracks, we see that the three Slocums assigned to these two tracks are uniformly spaced and, similarly, all six Slocums are still synchronized in two subgroups.

In the presence of disturbances such as flow, the GCCS regulates the glider progress around the track to achieve the desired along-track spacing between the gliders. For example, the control algorithm used during the Monterey Bay deployment steers gliders to inside (resp., outside) "lanes" on each track to speed up (resp., slow down). To evaluate the sampling performance of this algorithm, we compute the glider OA mapping error, shown in Fig. 5(a) and (b). In Fig. 5(c), we plot the sampling performance metric, which is the average of the OA mapping error, evaluated in the interior and on the boundary of the glider sampling domains (less error is better). When we adapted the GCT, we effectively reduced the sampling effort in the original domain; this adaptation increased the average error in the domain by about 5%. However, measurements collected on the new track fill the gap in the OA mapping error in the center of the original southernmost track [to see this, compare the grayscale map in Fig. 5(b) and (a)].

The GCCS supports GCT adaptations to improve collective mapping performance. We quantify the effect of adapting the Monterey Bay GCT by computing an additional metric, called the percentage metric, which is the percentage (of the interior or boundary) of the sampling domain that has mapping error less than a threshold of 0.5 (higher percentage is better). As shown in Fig. 5(c), the percentage metric shows a degradation of the sampling performance inside the box after the adaptation, but no degradation of performance on the boundary. That is, the interior area percentage metric exhibits downward fluctuations after the GCT was adapted, whereas the boundary percentage metric appears unaffected.

B. *Real Glider Deployment in Buzzards Bay*

In collaboration with Dr. D. Fratantoni of WHOI, the GCCS controlled two Slocum gliders in a GCCS sea trial in Buzzards Bay in March 2006 [17]. The gliders travelled clockwise around a single rectangular track with dimensions 2.8 km $\times$ 5.6 km. In addition, the GCCS sought to maintain a fixed, along-track separation distance of 1/6 the track perimeter, which corresponds to a curve phase of approximately 1 rad. The Buzzards Bay GCT is shown in Fig. 2(b). In this section, we summarize results from three days of coordinated control of the two gliders to this GCT. Additional analysis and a description of the control algorithm appear in [18].

During the Buzzards Bay deployment, coordination of the gliders was difficult due to strong tidal flow. Fig. 5(d) and (e) shows the glider trajectories superimposed on gridded OA flow maps computed from their measurements. During the deployment, the ocean currents were highly variable in space and time. We estimated the velocity decorrelation lengths to be 2.5 km (spatial) and 3 h (temporal). In Fig. 5(d), the gliders have good separation, but strong northeastern flow degrades their ability to stay on the prescribed track. In Fig. 5(e), both the separation and track-following performance are poor due to strong westward flow, which exceeded the glider effective speed. Fig. 5(f) shows the gliders recovered the desired curve-phase separation at the end of the third day.

This experiment demonstrates both the capabilities and limitations of the GCCS in a real glider deployment with strong flow. During periods of moderate flow, we observe good system performance in terms of track following and glider coordination. During periods of extreme flow, the system performance degrades substantially. We are incorporating a flow model into the GCCS to improve coordination performance in strong currents. In such situations, however, adaptation of the glider coordinated trajectories is often necessary. For example, the predominant flow conditions can dictate the direction of travel around the track and even the location and orientation of the track. Currently, GCT adaptation requires human intervention. Automated adaptation is an exciting challenge.

V. Summary and Conclusion

Autonomous underwater gliders are a reliable platform for long-duration ocean sampling with multiple vehicles. The GCCS implements real-time feedback control of a glider fleet to a set of coordinated trajectories. During each GCCS planning cycle, we predict glider motion using a detailed, 3-D model and generate future trajectories using a simple, planar model. A combination of good track planning and good real-time coordination achieves high sampling performance, as indicated by the OA mapping error and corresponding metrics. We describe two GCCS demonstrations: one with ten (virtual) gliders and the other with two gliders.

The GCCS demonstrations justify using feedback control of a high-level, simple model for automated, real-time trajectory planning of a fleet of autonomous vehicles. Both the Monterey Bay and Buzzards Bay deployments underscore the importance of choosing and adapting the planned glider coordinated trajectories in response to flow conditions and fleet sampling performance. We demonstrated the value of the GCCS simulation testbed by identifying and addressing inefficiencies in the Spray glider configuration during the Monterey Bay virtual deployment. The Buzzards Bay experiment motivates our ongoing work on improved robustness of coordinated control algorithms in adverse flow conditions. In August 2006, the GCCS coordinated six Slocum gliders for over three weeks during the ASAP deployment. For a description and analysis of these promising results, see [19].

Acknowledgment

The authors would like to thank F. Lekien, P. Bhatta, D. Gurkins, and J. Pinner of Princeton University, Princeton, NJ; D. Fratantoni and J. Lund of Woods Hole Oceanic Institution (WHOI), Woods Hole, MA; R. Davis, J. Sherman, and B. Jones of Scripps Institution of Oceanography (SIO), La Jolla, CA; P. Lermusiaux, W. Leslie, and P. Haley of Harvard University, Harvard, Cambridge, MA; and the rest of the ASAP team.

References

[1] N. E. Leonard, D. A. Paley, F. Lekien, R. Sepulchre, D. M. Fratantoni, and R. E. Davis, "Collective motion, sensor networks and ocean sampling," *Proc. IEEE*, vol. 95, no. 1, pp. 48–74, Jan. 2007.

[2] E. Fiorelli, N. E. Leonard, P. Bhatta, D. A. Paley, R. Bachmayer, and D. M. Fratantoni, "Multi AUV control and adaptive sampling in Monterey Bay," *IEEE J. Ocean. Eng.*, vol. 31, no. 4, pp. 935–948, Oct. 2006.

[3] T. B. Curtin, J. G. Bellingham, J. Catipovic, and D. Webb, "Autonomous oceanographic sampling networks," *Oceanography*, vol. 6, no. 3, pp. 86–94, 1993.

[4] E. Creed, J. Kerfoot, C. Mudgal, S. Glenn, O. Schofield, C. Jones, D. Webb, and T. Campbell, "Automated control of a fleet of Slocum gliders within an operational coastal observatory," in *Proc. MTS/IEEE Conf. OCEANS*, 2003, vol. 2, pp. 726–730.

[5] B. Schulz, B. Hobson, M. Kemp, and J. Meyer, "Field results of multi-UUV missions using Ranger micro-UUVs," in *Proc. MTS/IEEE Conf. OCEANS*, 2003, vol. 2, pp. 956–961.

[6] S. S. Mupparapu, S. G. Chappell, R. J. Komerska, D. R. Blidberg, R. Nitzel, C. Benton, D. O. Popa, and A. C. Sanderson, "Autonomous systems monitoring and control (ASMAC)—An AUV fleet controller," in *Proc. IEEE/OES Autonom. Underwater Veh. Workshop*, Jun. 2004, pp. 119–126.

[7] R. E. Davis, C. E. Eriksen, and C. P. Jones, , G. Griffiths, Ed., "Autonomous buoyancy-driven underwater gliders," in *The Technology and Applications of Autonomous Underwater Vehicles*. New York: Taylor and Francis, 2002, ch. 3, pp. 37–58.

[8] R. Sepulchre, D. A. Paley, and N. E. Leonard, "Stabilization of planar collective motion: All-to-all communication," *IEEE Trans. Autom. Control*, vol. 52, no. 5, pp. 811–824, May 2007.

[9] R. Sepulchre, D. A. Paley, and N. E. Leonard, "Stabilization of planar collective motion with limited communication," *IEEE Trans. Autom. Control* [Online]. Available: http://www.princeton.edu/~naomi, to be published

[10] F. Zhang and N. E. Leonard, "Coordinated patterns on smooth curves," in *Proc. IEEE Int. Conf. Netw. Sens. Control*, 2006, pp. 434–440.

[11] D. A. Paley, N. E. Leonard, and R. Sepulchre, "Collective motion of self-propelled particles: Stabilizing symmetric formations on closed curves," in *Proc. 45th IEEE Conf. Decision Control*, San Diego, CA, Dec. 2006, pp. 5067–5072.

[12] D. L. Rudnick, R. E. Davis, C. C. Eriksen, D. M. Fratantoni, and M. J. Perry, "Underwater gliders for ocean research," *Mar. Technol. Soc. J.*, vol. 38, no. 1, pp. 48–59, 2004.

[13] P. F. J. Lermusiaux, "Adaptive modeling, adaptive data assimilation and adaptive sampling," *Physica D*, vol. 230, no. 1–2, pp. 172–196, 2007.

[14] F. P. Bretherton, R. E. Davis, and C. B. Fandry, "A technique for objective analysis and design of oceanographic experiments applied to MODE-73," *Deep Sea Res.*, vol. 23, pp. 559–582, 1976.

[15] Princeton University, "Adaptive sampling and prediction," Princeton, NJ, 2006 [Online]. Available: http://www.princeton.edu/~dcsl/asap

[16] Harvard University, "Adaptive sampling and prediction," Cambridge, MA, 2006 [Online]. Available: http://oceiins.deas.harvard.edu/asap/index-asap.html

[17] D. M. Fratantoni and J. M. Lund, "Glider operations in Buzzard's Bay, MA," Woods Hole Oceanic Inst., Woods Hole, MA, Tech. Rep. BUZZ0306, 2006 [Online]. Available: http://asl.whoi.edu/research/gods/datrep/buzi0306.datrep.pdf

[18] F. Zhang, D. M. Fratantoni, D. A. Paley, J. M. Lund, and N. E. Leonard, "Control of coordinated patterns for ocean sampling," *Int. J. Control* vol. 80, no. 7, pp. 1186–1199, 2007.

[19] D. A. Paley, "Cooperative control of collective motion for ocean sampling with autonomous vehicles" Ph.D. dissertation, Dept. Mech. Aerosp. Eng., Princeton Univ., Princeton, NJ, Sep. 2007 [Online]. Available: http://www.princeton.edu/~dpaley/papers/paley-thesis.pdf